Height-dependent sunrise and sunset: Effects and implications of the varying times of occurrence for local ionospheric processes and modelling

Tobias G.W. Verhulst *, Stanimir M. Stankov

Royal Meteorological Institute (RMI), Ringlaan 3, B-1180 Brussels, Belgium

Abstract

It is well established that the sunrise and sunset periods are of particular importance to ionospheric research and modelling because of the rapid changes in the ionospheric plasma density, temperature, and dynamics. In particular, the sharp increase in the ionisation following sunrise results in a quick increase in the ionospheric peak density, N_mF_2, and a decrease in the peak height, h_mF_2. Changes in plasma temperature, scale height and transport processes add further complexity which makes it difficult to investigate and model the ionospheric behaviour during this transitional period from night to day. One of the aspects contributing to this difficulty is that not all ionospheric altitudes are exposed to the first sunlight of the day at the same time. During sunrise, the upper part of the ionosphere is illuminated prior to the lower part which is still in the dark. The boundary between sunlit and dark regions moves downwards until it reaches the surface of the Earth, which is commonly taken as the moment of sunrise at certain geographical coordinates. This means that the sunrise at surface level does not occur until after the entire ionosphere has been illuminated. During sunset, the same process happens in reverse order. This paper addresses the issue of these altitude-dependent times of sunrise and sunset and reports on our study of some of the effects on the diurnal variations in the ionospheric characteristics.

1. Introduction

The ionisation of the neutral particles in the upper atmosphere is primarily the result of photoionisation caused by solar irradiation. The contribution of transport processes to the ion and electron density depends strongly on altitude. At higher altitudes, transport processes have sufficient influence to maintain of the F layer throughout the night, while at lower altitudes, in the E and D regions, the transport processes are rather insignificant and are usually ignored. The amount of local photoionisation is commonly described by the Chapman production function, which is well known in the literature—see, for example, Schunk and Nagy (2000). This production function depends, among other things, on the solar elevation angle.

The LIEDR (Local Ionospheric Electron Density profile Reconstruction) model has been developed and used to reconstruct the local electron density profile for the entire ionosphere (see Fig. 1), including the topside (Stankov et al., 2011). This is a real time model, based on the ionosonde characteristics automatically scaled from ionograms, as well as GNSS derived total electron content (*TEC*). In the current work, we use this model to reconstruct the electron density above the Dourbes ionosphere observatory,

* Corresponding author.
  E-mail addresses: tobias.verhulst@oma.be (T.G.W. Verhulst), s.stankov@meteo.be (S.M. Stankov).
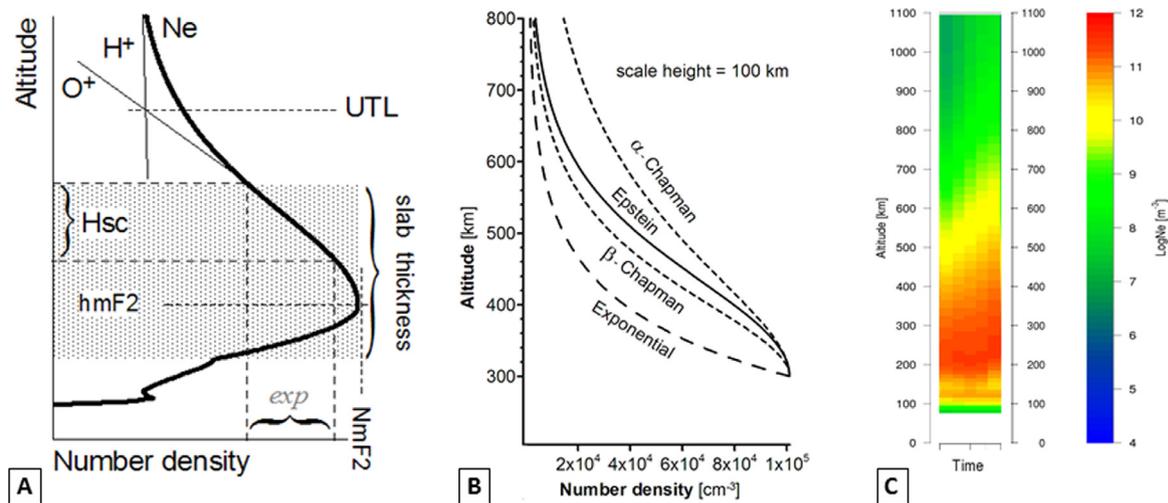
Fig. 1. Panel (A): Schematic of the vertical ionospheric ion and electron density profiles, indicating key characteristics such as peak density (N_mF_2), peak density height (h_mF_2), plasma scale height (H_{sc}), and the ionospheric slab thickness. Panel (B): Comparison between vertical density profiles obtained with basic analytical models for a given scale height of 100 km. Panel (C): A sample of five profilograms produced in the course of one hour; each profilogram shows the electron density, N_e (colour-coded, logarithmic scale on right) as a function of altitude (vertical axis) and time (horizontal axis). (For interpretation of the references to color in this figure legend, the reader is referred to the web version of this article.)

located at 50.1°N and 4.6°E. The LIEDR operational results can be found on the web-page http://ionosphere.meteo.be/ionosphere/liedr. At the Dourbes observatory, a Digisonde DPS4D digital ionosonde (Reinisch et al., 2009) and a NovAtel GPStation-6 GNSS receiver are co-located, providing all the necessary input data for the LIEDR model.

A major problem for the reconstruction of the complete electron density profile is that, while the ionosonde can be used to obtain the bottom-side characteristics, little information is directly available for the topside ionosphere (Fig. 1). The topside *TEC* can be calculated from the total GNSS-derived *TEC* by subtracting the bottom-side *TEC* estimated from the bottom-side electron density profile reconstructed from ionosonde measurements. However, to be able to deduce the topside electron density profile from the topside *TEC*, a suitable profiler function must be chosen. In the LIEDR model, a Chapman profile, Epstein profile, and exponential profile are available to model the topside. The model can switch between different profiler functions depending on various parameters like time of day, season, geomagnetic conditions, etc. (Verhulst and Stankov, 2014, 2015).

However, at different altitudes, the ionosphere is not only exposed to the solar irradiation at different zenith angles but is also exposed to the irradiation at different times during the sunrise and sunset periods. Simply switching between different, fixed topside profiles for day and night might therefore not be sufficient to accurately model the ionosphere. Some proposed improvements are to use a combination of various profiles, with different scale heights at different altitudes (Fonda et al., 2005; Kutiev et al., 2006), or to use a profile with an altitude dependent scale height (Reinisch et al., 2007; Nsumei et al., 2012). The general idea of those methods is to improve the topside modelling by using a different profile function at different

altitudes. In this work we demonstrate a different, but conceptually similar, approach: we switch between the fixed profiles available in the LIEDR model, but we use different profiles for the parts of the ionosphere which are sunlit and the parts that are in darkness. This means that our method, too, is using different profiles at different altitudes. The main distinction with the methods described in the aforementioned literature is that we base our choice of profile function on the position of the sun alone, instead of historical or real-time data.

This paper is organised as follows. First, we derive the relevant mathematical formulas and computational algorithms than can be used to calculate which part of the ionosphere is irradiated by the sun at a given time and place. After this, we show various ionosonde observations, and discuss their relation to the varying times of sunrise at different altitudes. Finally, we show how the LIEDR model can be improved by adapting the topside profiles to the height dependent sunrise and sunset.

2. Theoretical considerations

2.1. Height of the permanently sunlit region above a certain location

At a certain altitude above the Earth's surface, depending on the day of year and the latitude, the solar nadir is above the horizon. If this height ($h_\odot$) is in the ionosphere, i.e. below the upper O^+/H^+ ion transition level (UTL), a part of the ionosphere would remain sunlit throughout the night. This means that photoionisation, and plasma transport, would continue to take place in the ionosphere similarly to the daytime conditions. This is particularly important if $h_\odot$ is at (lower) altitudes where the photoionization becomes more significant. The issue is of
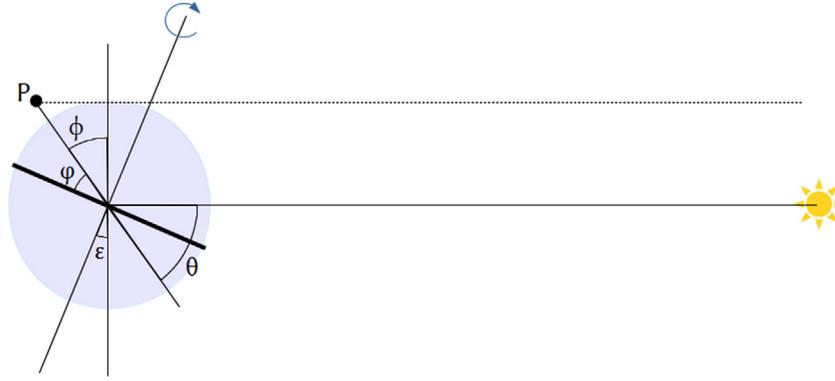
Fig. 2. An observer at point *P*, at some altitude above the Earth's surface at latitude φ, sees the sun exactly on the horizon (ignoring breaking of light in the atmosphere, which is not very important for the ionising fraction of the spectrum). For an observer at the same latitude at sea level, the sun is below the horizon.

importance with regard to modelling the topside ionosphere, since it is the topside ionosphere that remains exposed to the solar irradiation for much longer periods.

At midnight during summer solstice, assuming that the sunlight arrives at the Earth parallel to the ecliptic and that the Earth is spherical, the height $h_\odot$ above the Earth's surface can be derived from the following equation:

$$\left(R_{\oplus} + h_\odot\right)\cos\phi = R_{\oplus} \tag{1}$$

where $R_{\oplus}$ is the Earth's radius and $\phi = \frac{\pi}{2} - \theta$ (see Fig. 2). From this equation, it follows that

$$h_\odot = R_{\oplus}\frac{1 - \cos\phi}{\cos\phi} \tag{2}$$

$$= R_{\oplus}\frac{1 - \sin\theta}{\sin\theta} \tag{3}$$

or, with $\theta = \varphi + \varepsilon$ (where φ is the latitude and $\varepsilon = 22.44° = 0.3917$ is the obliquity angle):

$$h_\odot(\varphi) = R_{\oplus}\frac{1 - \sin(\varphi + \varepsilon)}{\sin(\varphi + \varepsilon)} \tag{4}$$

In order to obtain a formula for days other than at summer solstice, the solar declination $\delta_\odot$ needs to be used instead of the obliquity angle. If assuming the orbital eccentricity of the Earth to be zero, and using the following approximation

$$\arcsin(\sin\alpha\cos\beta) \approx \alpha\cos\beta, \tag{5}$$

the result would be the following formula for $h_\odot$:

$$h_\odot = R_{\oplus}\frac{1 - \sin\left(\varphi + \varepsilon\cos\left(\epsilon - \frac{\pi}{2}\right)\right)}{\sin\left(\varphi + \varepsilon\cos\left(\epsilon - \frac{\pi}{2}\right)\right)}, \tag{6}$$

in which ϵ is the ecliptic longitude. The ecliptic longitude is given (approximately) by

$$\epsilon - \frac{\pi}{2} = f \cdot n$$

with n the number of days past winter solstice and $f = \frac{2\pi}{365.24}$. Thus,

$$h_\odot(\varphi, n) = R_{\oplus}\frac{1 - \sin(\varphi + \varepsilon\cos(f \cdot n))}{\sin(\varphi + \varepsilon\cos(f \cdot n))} \tag{7}$$

Fig. 3A shows this height as a function of latitude for the summer and winter solstices in the Northern Hemisphere. The summer curve reaches an altitude of zero at 66.56°, which is indeed the latitude of the polar circle.

A slightly more accurate formula can be obtained by not using the above approximation (5) but instead using the following expression for the solar declination $\delta_\odot$:
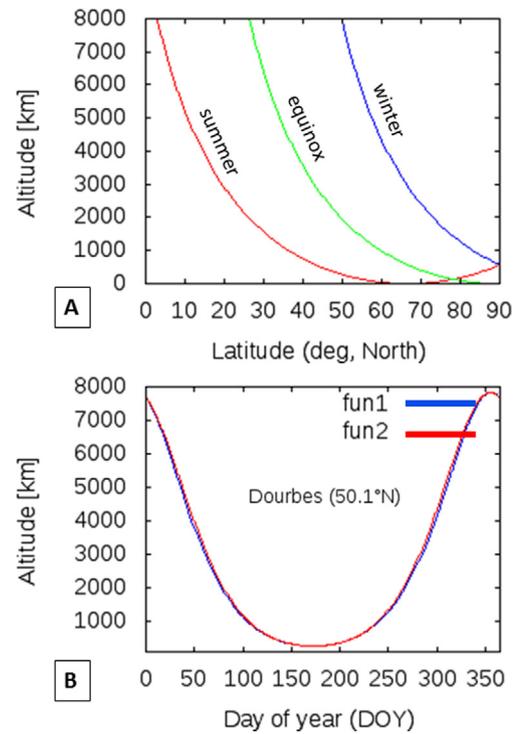
Fig. 3. Panel A: The lowest height of the permanently sunlit atmosphere for equinox and for winter and summer solstices as a function of latitude (Ref. Northern Hemisphere). Panel B: The lowest height of the permanently sunlit atmosphere above Dourbes, as calculated with formulas (7) (blue) and (9) (red), for each day of the year (DOY). (For interpretation of the references to color in this figure legend, the reader is referred to the web version of this article.)

$$\delta_\odot = \arcsin\left(\sin\varepsilon \cdot \cos\left(fn + 2e\sin\left(f(n-12)\right)\right)\right) \quad (8)$$

(where n is the days past winter solstice and $e = 0.0167$ is the eccentricity of the Earth's orbit). The height of the permanent sunlight is then given by

$$h_\odot(\varphi, n) = R_\oplus \frac{1 - \sin\left(\varphi + \arcsin\left(\sin\varepsilon \cdot \cos\left(fn + 2e\sin\left(f(n-12)\right)\right)\right)\right)}{\sin\left(\varphi + \arcsin\left(\sin\varepsilon \cdot \cos\left(fn + 2e\sin\left(f(n-12)\right)\right)\right)\right)} \quad (9)$$

In Fig. 3B both, the approximate height given by (7) and the more accurate height given by (9), are plotted for the location of the Dourbes ionosonde station (50.1°N, 4.6° E). It can be seen from the figure that the difference between both versions is negligible, which justifies the use of the simpler expression (7).

2.2. Sunrise and sunset as a function of height

The next issue to consider is at what times, given the day of year, the sun will appear and disappear at a given altitude above sea-level. We call this the altitudinal solar terminator. Algorithms exist to calculate at what times the sun is at a certain angle above or below the geometric horizon (Nautical Almanac Office, 1990; Meeus, 1985, 1998; Jenkins, 2013). Besides the definition of sunrise and sunset as the moment when the midpoint of the sun is 90° from zenith, several other angles have historically been used. The official twilight is considered to be the moment when the centre of the sun is 90.83° from zenith, which is the moment when the entire solar disk is below the horizon. Civil, nautical and astronomical twilight are defined as

the moment when the sun is respectively 6°, 12° and 18° below the horizon.

Here, we introduce a new type of twilight: Kármán twilight, defined as the moment the sun is below the horizon as seen from the Kármán line (100 km above sea level). Since this is the altitude of the bottom of the ionosphere, the Kármán twilight marks the period of transition between an ionosphere entirely lit by the sun and an ionosphere entirely in the dark.

Implementations of the algorithms for the sunrise and sunset times exist in standard libraries and packages in various programming languages. For example, for Python there are package `sun` and `astral` that provide this capability. However, in order to have absolute control over the details of the implementation, we have written the necessary code ourselves in Python. This code can be found in the supplementary material to this paper.

3. Observed influences of high-altitude sunrise and sunset

3.1. Influence on the E layer

It is well known that the ionisation in the E region is almost exclusively the result of local photo ionisation, with only a small contribution from transport processes. The E layer appears right after sunset, and disappears shortly after the irradiation has ceased. Therefore, to understand and model the various parameters characterising the E layer, the effect of the different times of sunrise at different altitudes has to be taken into account (see Fig. 4).
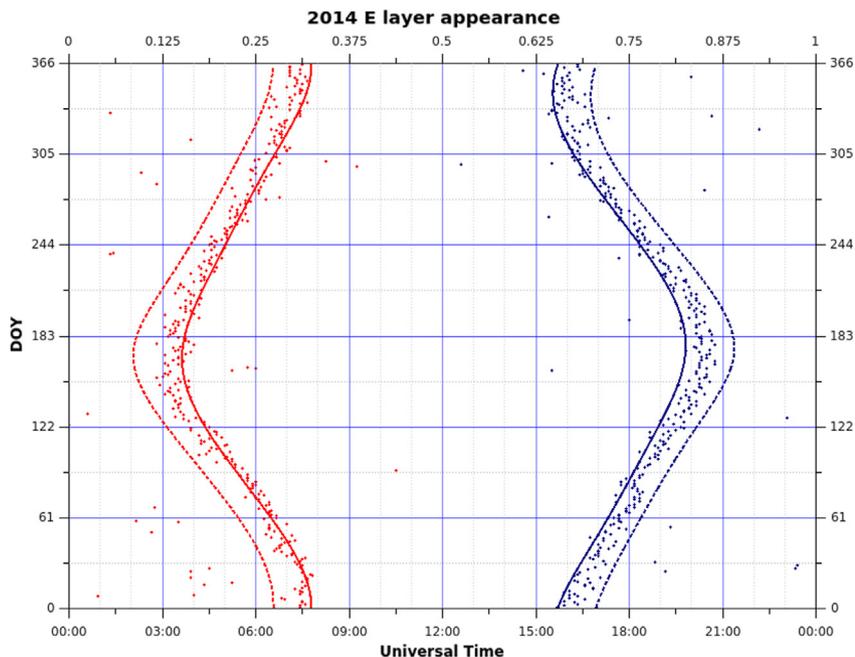
Fig. 4. The times of the first (red dots) and last (blue dots) detections of the E layer above Dourbes for each day of year 2014, approximated at sea level (solid curves) and at an altitude of 100 km (dashed curves). (For interpretation of the references to color in this figure legend, the reader is referred to the web version of this article.)

In Fig. 5A and B the average values of the *E*-layer critical frequency f_oE and virtual height $h'E$ are plotted for each season. As expected, the *E* layer appears in the morning, and the density increases until noon, when the irradiation is maximal, before gradually decreasing until the layer disappears in the evening. It can be seen in Fig. 5B that the peak of the *E* layer is not at a fixed altitude. Throughout the morning, the peak altitude decreases, and after noon starts increasing again. Although this change in peak height is small, of the order of 5 km over the day, it is a significant effect of the change throughout the day of the solar elevation angle. With the changing elevation angle, the altitude where the photoionisation is maximal changes as well. It is evident that the seasonal differences in the solar elevation angle have significant effects on the *E*-layer characteristics.

Not only is the peak density lower in winter and higher in summer, but also the peak height shows a clear seasonal dependency. Additionally, in Fig. 5C, the number of detections of the presence of an *E* layer is plotted for each seasons. From this, it is clear that the appearance and disappearance of the *E* layer happen very suddenly.

3.2. Height-dependent solar irradiance and F-layer characteristics

Fig. 6 shows the times of sunrise and sunset at different altitudes during the year, again calculated for the location of the Dourbes ionosonde. The boundary of the permanently sunlit region during midsummer night is at 377 km altitude. It can be seen in Fig. 7 that the largest altitude
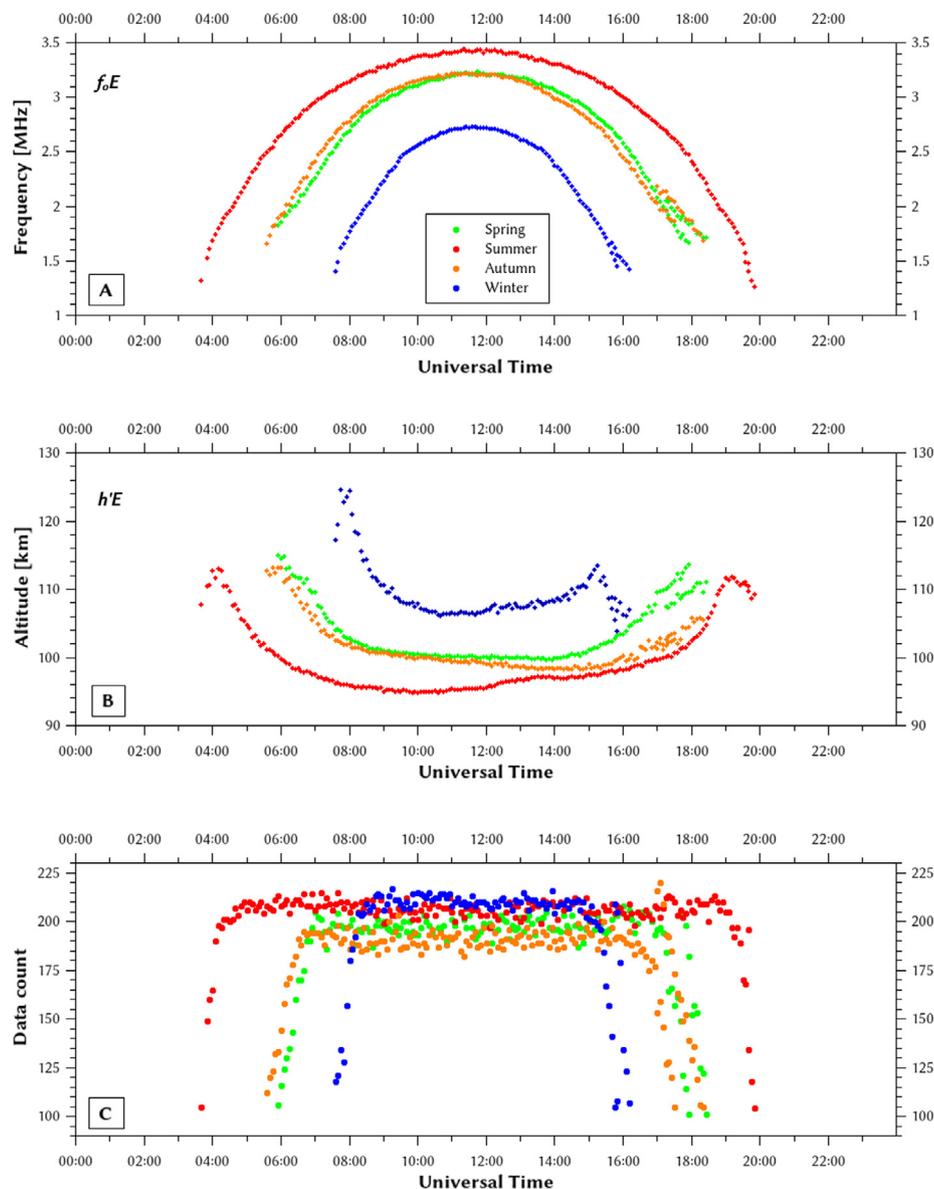
Fig. 5. Average diurnal behaviour of the *E*-layer critical frequency f_oE (panel A) and (virtual) height $h'E$ (panel B) at different seasons as measured by the Dourbes digisonde. Panel (C): Number of days during which an E layer was detected from ionosonde measurements (5-min cadence) at Dourbes at the times of the soundings, plotted separately for each of the four seasons.
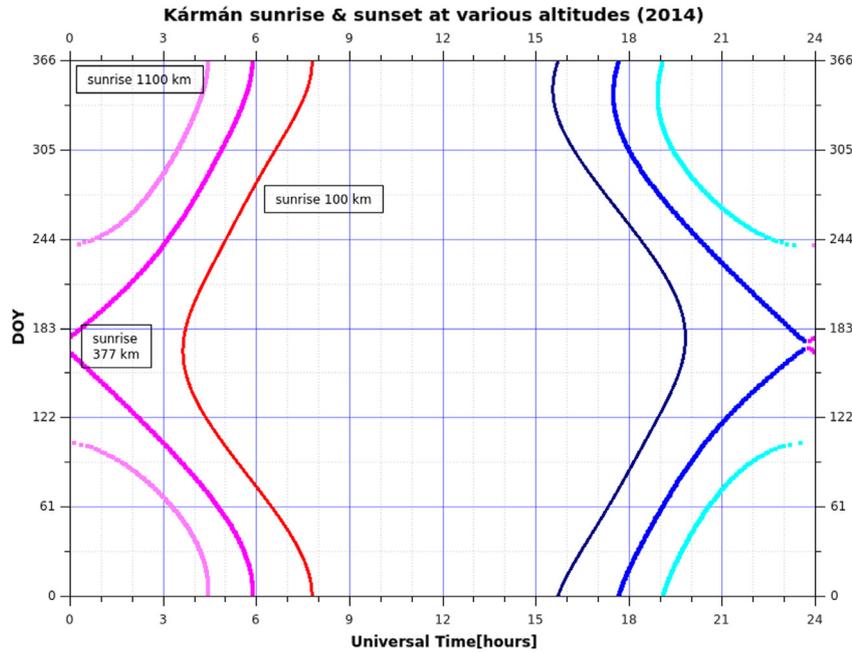
Fig. 6. Sunrise and sunset times as a function of DOY at different altitudes above Dourbes (50.1°N,4.6°E), as calculated for year 2014.
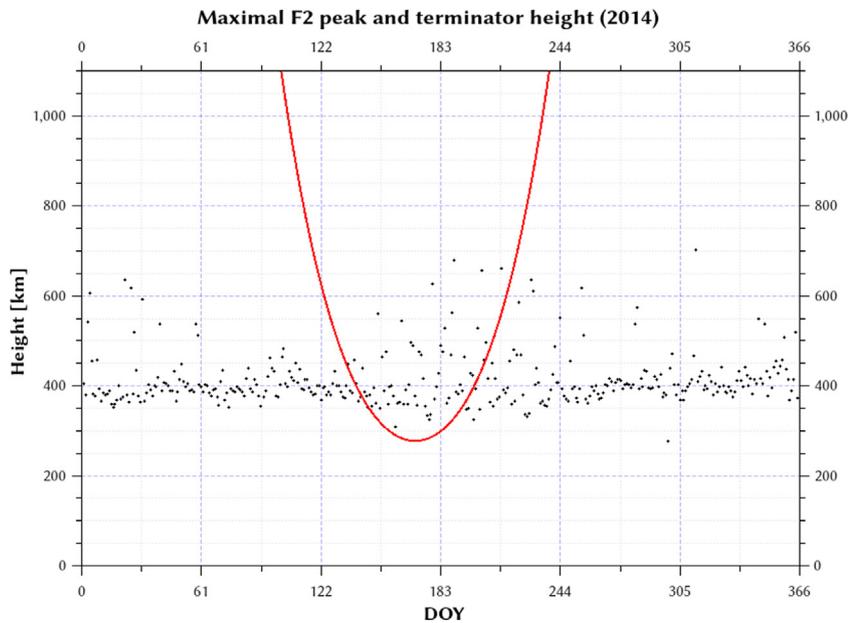
Fig. 7. The daily maximal height of the F_2 peak (black dots) and the boundary of the permanent sunlight (red line) during 2014. (For interpretation of the references to color in this figure legend, the reader is referred to the web version of this article.)

of the F_2 peak during the night is around 400 km. It is evident from this same figure that for several months around the summer solstice the topside ionosphere is for a large part, or even in its entirety, being irradiated by the sun throughout the entire day. Nevertheless, there is no evidence of the maximal peak height itself being influenced by the seasonal variation of the solar terminator height. The daily maximum is stable around the same altitude of 400 km throughout the entire year.

In Fig. 8 the time of the first appearance of the E layer and the time of the minimum in the critical frequency f_oF_2 are shown, throughout one year. Since the electron density decreases throughout the night, until photoionisation resumes at sunrise, the minimum in the critical frequency can be expected to occur shortly before sunrise. As already mentioned, the E layer is almost exclusively produced by local photoionisation and is therefore expected to appear just after sunrise. Nevertheless, it is clear from the picture
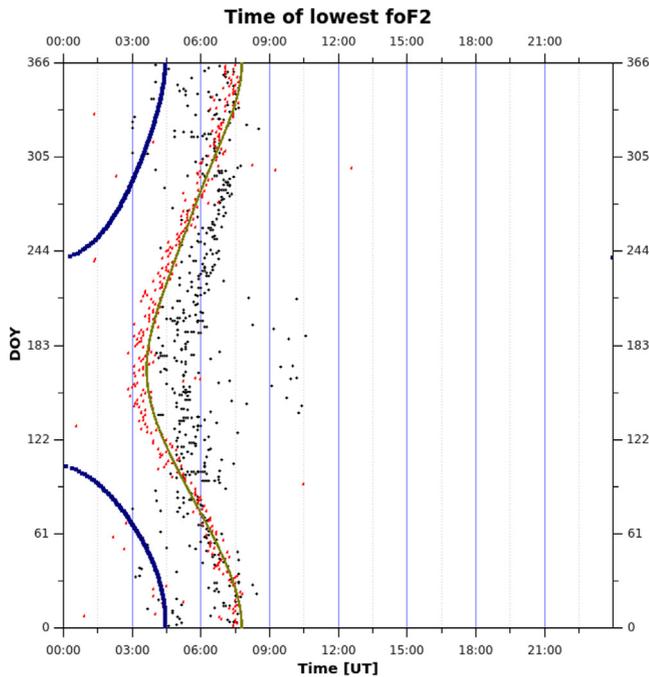
Fig. 8. The times of the daily minima for the critical frequency f_oF_2 (blue dots) and the first appearances of the E layer (red dots) during 2014. The solid lines show the time of sunrise at 90 km (green) and 1100 km (blue). (For interpretation of the references to color in this figure legend, the reader is referred to the web version of this article.)

that, on most days, the appearance of the E layer happens before the critical frequency reaches its minimum.

4. Adaptation of the LIEDR model

Ionospheric characteristics, scaled automatically from ionosonde measurements together with vertical TEC values calculated from GNSS measurements, are used as input for the RMI Local Ionospheric Electron Density Reconstruction (LIEDR) system (Stankov et al., 2011). LIEDR uses $f_oF_2, f_oE, M(3000)F_2$ and TEC as input parameters, as well as solar radio flux and geomagnetic measurements. It acquires and processes in real time the concurrent and collocated ionosonde and GNSS TEC measurements, and ultimately, deduces a full-height electron density profile based on a reconstruction technique (Stankov et al., 2003) utilising different ionospheric profiles (Exponential, Epstein, Chapman) and empirically-modelled values of the O^+–H^+ ion transition height. In this way, the topside profile is more adequately represented because of the use of independent additional information about the topside ionosphere. The retrieval of the electron density distribution is performed in two main stages: construction of the bottomside electron profile (below h_mF_2) and construction of the topside profiles (above h_mF_2). The ionosonde measurements are used for directly obtaining the lower part of the electron density profile. The corresponding bottomside part of TEC is calculated from this profile and is then subtracted from the entire TEC in order to obtain the

unknown portion of TEC in the upper part. The topside TEC is used in the next stage for deducing the topside ion and electron profiles. The result is a full-height profile of the electron density distribution, from 90 km up to about 1100 km, which can be easily put on display (profilogram) for a close-up analysis (Fig. 1).

The choice of an appropriate topside profile for use in the LIEDR is an important issue, which is still the subject of ongoing research (Verhulst and Stankov, 2013, 2014, 2015). In the currently operational version of the model, different profile functions are selected for use during daytime and night-time, respectively: an exponential profile is used during the day, while the Epstein profile is used at night. However, if the time of change between two topside profiles is based on the time of sunrise and sunset at sealevel, artefacts appear in the reconstructed profilograms. In practice, the most obvious discontinuities appear in the evening, when switching to the nigh-time profile—see Fig. 9, top panel. A possible solution is to switch the topside profile at the times of sunrise and sunset at the Kármán altitude. An example of this is shown in the middle panel of Fig. 9. The discontinuity clearly visible in the top panel is not so obvious in this case, and also happens slightly later (since the sun sets later at higher altitude).

Another possibility is switching the profiles not based on the sunrise and sunset at a fixed altitude, but at the altitude of the F_2 peak. This way, regular variations of the ionospheric conditions with season and solar activity, as well as exceptional conditions due to geomagnetic storms, can automatically be taken into consideration in determining the time of the switch. This is the method currently implemented in the operational LIEDR model, and an example is shown in the bottom panel of Fig. 9.

Fig. 10 shows the output of the LIEDR model for a week in each season, as well as the altitude of the solar terminator during these periods. It is evident from this figure that the effect of the height dependency of the solar terminator at this location is most important during the summer. Depending on the exact altitude of the F_2 peak, there can be some nights during which there will be no transition to the night-time profile at all.

5. Discussion

Sunrise and sunset periods are of particular importance to ionospheric research and modelling because of the rapid changes in the key ionospheric plasma characteristics, such as the ion/electron densities and temperature, as well as in the dynamics of the plasma transport processes. In particular, the sharp increase in the ionisation following sunrise leads to a prompt and substantial increase in the ionospheric peak density, N_mF_2, and a decrease in the peak height, h_mF_2. Changes in the temperatures and scale heights for both the neutral and ionised components, accompanied by active plasma transport, add further complexity which makes it difficult to investigate and model the ionospheric behaviour during these transitional periods from night to
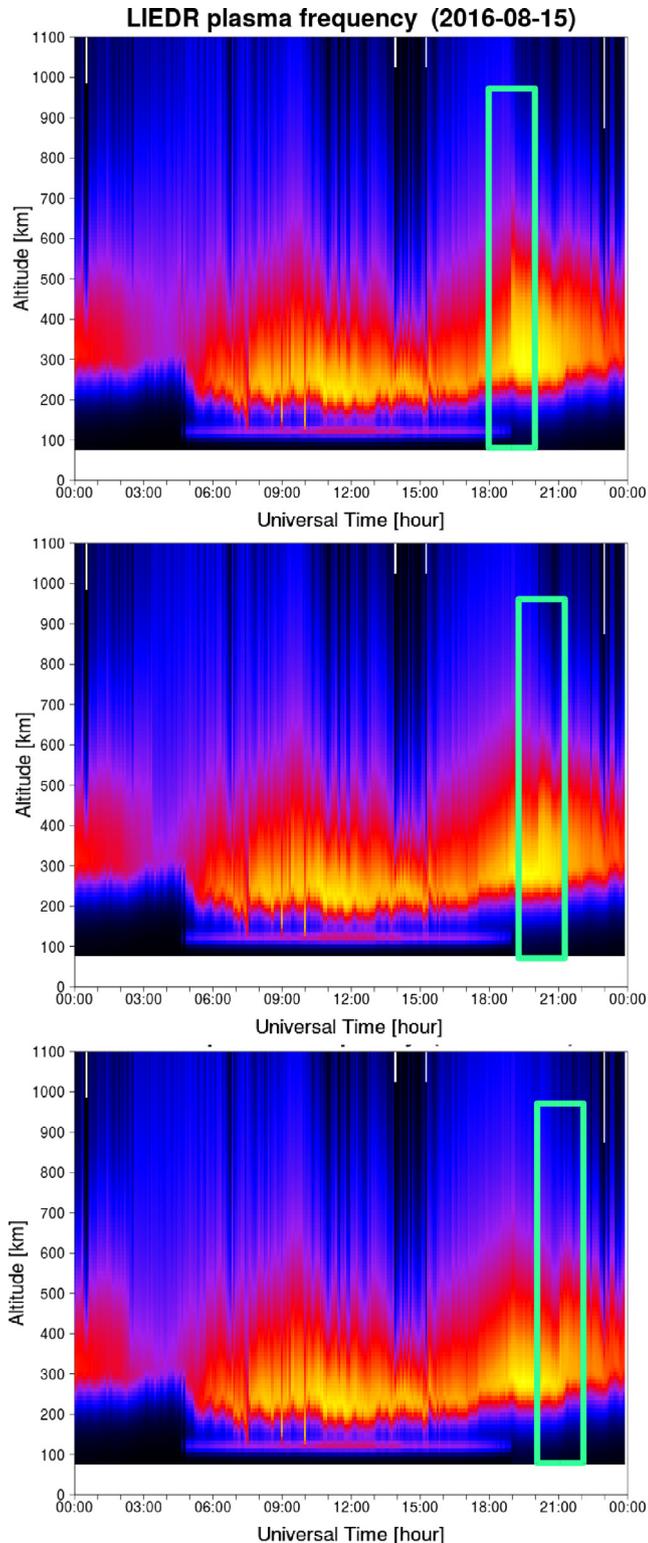
Fig. 9. Plasma frequency representation of the LIEDR output calculated for 15 August 2016 using the measurements from Dourbes. The top-panel was produced switching between day-time and night-time profiles based on the times of sunrise and sunset at sea-level, the middle panel using the times at a fixed 100 km altitude, and the bottom panel using the times at the F_2 peak altitude. An artificial discontinuity in the profilograms happening around sunset is marked by a rectangle.

day and day to night. One of the aspects contributing to this difficulty is that not all ionospheric altitudes are exposed to the sunlight at the same time.

Therefore, when using ionospheric databases, whether for analysing a certain phenomenon or for building an empirical model, it is quite often necessary to bin the data according to day-time or night-time conditions. Such separation however does not necessarily mean sunlit for day-time and dark for nigh-time. For example, during summer in the Northern hemisphere, there is a part of the ionosphere, above a certain altitude, that is constantly sunlit even during the nominal night. This poses difficulties when creating a clean dataset for a proper analysis and modelling of the day-time and night-time conditions. The appropriate definition of what constitutes day and night at a given location varies not only throughout the year (see Fig. 5), but is also different for various ionospheric characteristics (see Fig. 8). In the latter figure, what should be considered day-time conditions for the E and F regions are shown to be slightly different.

Another example of the difficulty in distinguishing between day-time and night-time comes from the use of the model for reconstructing the electron density profile in the ionosphere above a certain location. In order to select the most appropriate empirical topside profile, it is the solar irradiation, or lack thereof, in the topside that needs to be taken into account, rather than the nominal day or night at ground level. As can be seen in Fig. 9, the problem of discontinuities appearing in the profilograms when switching from the day-time profile to the night-time profile can be substantially alleviated by switching between the profiles when the altitudinal solar terminator crosses the altitude of the main electron density peak.

However, even after implementing this improvement, small discontinuities in the profilograms may still appear during the transitional periods (see bottom panel of Fig. 9). This can now be readily understood: even at the time when the solar altitudinal terminator crosses the F_2 peak altitude, the highest parts of the topside are still fully irradiated by the sun. It means that, in these upper regions, the use of the night-time profile cannot deliver accurate results. Therefore, a further improvement to the LIEDR model would be to implement two different profiles—one for the sunlit part and another for the dark part of the ionosphere. This would be equivalent to introducing a topside profile which itself depends on the altitude (cf. Nsumei et al. (2012)). However, such implementation would require a change in the electron profile reconstruction methodology described in Section 4. Instead of dividing the vertical profile to bottomside and topside ionospheric parts only, this study suggests further dividing the vertical profile in the topside ionosphere by introducing lower topside and upper topside parts, thus accommodating the height of the sunlit ionosphere as well.
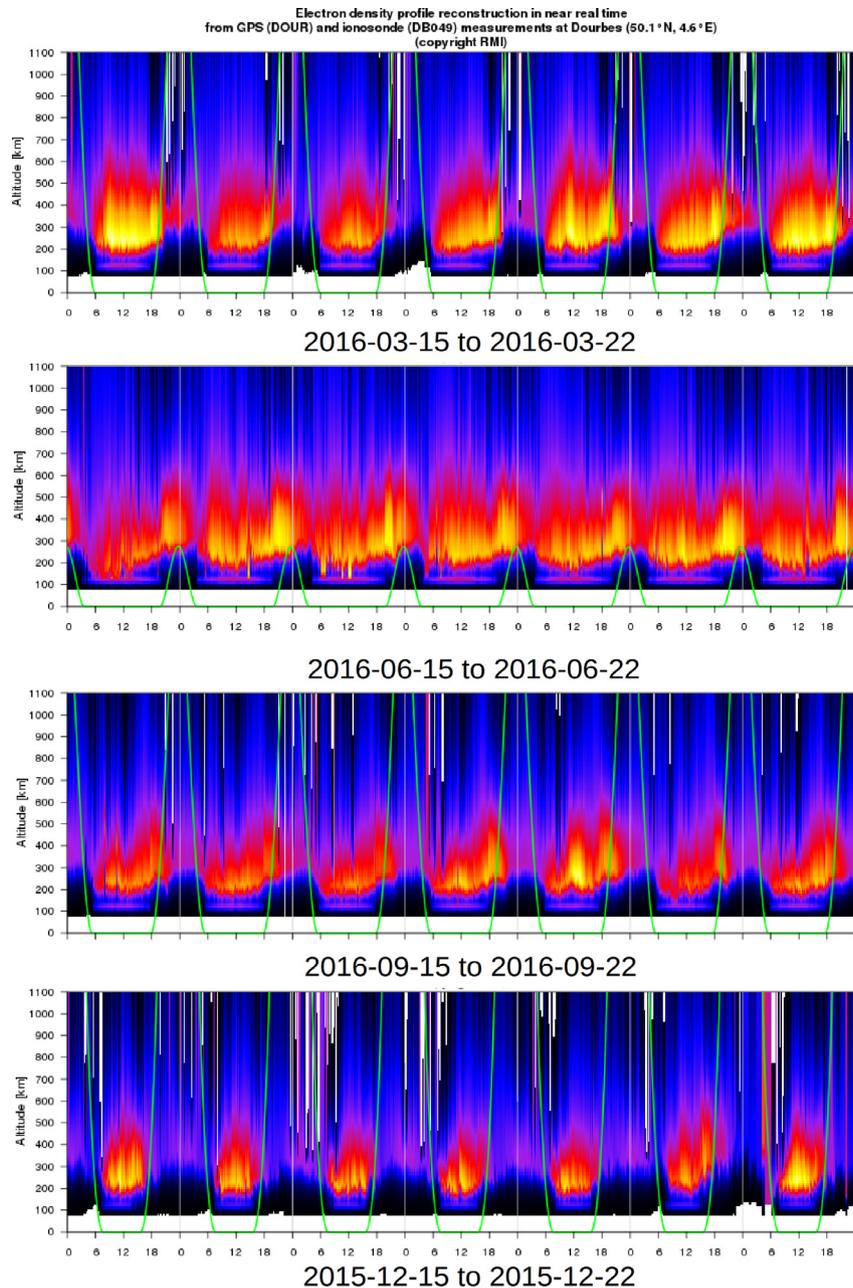
Fig. 10. Plasma frequency profilograms reconstructed using the improved LIEDR model above Dourbes for seven day around the equinoxes and solstices (top to bottom: spring, summer, fall, winter). The green line shows variation of the altitudinal solar terminator with time. (For interpretation of the references to color in this figure legend, the reader is referred to the web version of this article.)

As pointed out earlier in the discussion, the actual position of the altitudinal solar terminator is just one of several factors contributing to the difficulties in modelling the ionosphere during the dawn and dusk periods. In terms of ionospheric dynamics (Kelley, 2009), the mid-latitude F-layer is exposed to the complex interplay of plasma production and loss (dominant during day), neutral atmosphere winds, gravity and electromagnetic forces (dominant during night). Changes in dominance during the transitional periods, add further complexity to the modelling task. The ionospheric plasma drifts, both vertical and horizontal, are known to play a role in the plasma

redistribution processes occurring during these transition periods. Gravity and pressure gradients are mostly responsible for the vertical motion, while the neutral winds and electric fields are for the horizontal motion.

6. Conclusion

This paper is concerned with the complex issue of the solar illumination of the ionosphere at middle latitudes for different altitudes, time of day, and day of year. A common misconception is that above a certain location, night-time conditions are equivalent to dark conditions. There

are instances when, even at mid-latitudes, a part of the top-side ionosphere remains sunlit, at least partially and for various periods of time, during the statutory night (at middle latitudes, the period from sunset to sunrise at sea level). The lowest altitude above which the atmosphere is sunlit during night we termed as altitudinal solar terminator. Of particular concern are the sunrise and sunset periods when rapid changes occur in the ionospheric plasma composition and dynamics. Although the issue has always been known, it is still often overlooked or poorly handled most probably because of the complexities associated with calculating the exact position of the altitudinal solar terminator and implementing a relevant algorithm to minimise the errors caused by disregarding this issue.

The behaviour of the altitudinal solar terminator for the location of the Dourbes Observatory has been thoroughly investigated and the influence of the height-dependent sunrise and sunset on the ionospheric E and F layers presented here. Mathematical formulae have been deduced, and an algorithm developed, for calculating the height of the terminator as a function of the geographic latitude and the day of year. The algorithm has been successfully implemented in the operational LIEDR model that is used for reconstructing and imaging in real time the local ionospheric electron density profile. The implementation proved to be efficient in substantially improving the reconstruction by minimising, and in many cases even eliminating, the discrepancies between consecutive profiles that used to occur during sunset when switching from the LIEDR day-time to night-time profiles.

Several applications are envisaged for the formulae and algorithm presented. Perhaps the most important application would be in theoretical and empirical ionospheric models as demonstrated here. Another possible application would be in the development and use of comprehensive ionospheric/atmospheric databases. Scientific research can also be helped by ensuring the use of clean datasets leading to more reliable analyses.

Acknowledgement

Appendix A. Supplementary material

Supplementary data associated with this article can be found, in the online version, at http://dx.doi.org/10.1016/j.asr.2017.05.042.

References

Fonda, C., Coïsson, P., Nava, B., Radicella, S.M., 2005. Comparison of analytical functions used to describe topside electron density profiles with satellite data. Ann. Geophys. 48 (3), 491–495.

Jenkins, A., 2013. The Sun's position in the Sky. Eur. J. Phys 34, 633–652. Available from: <1208.1043v3>.

Kelley, M.C., 2009. The Earth's Ionosphere: Plasma Physics and Electrodynamics, second ed. Academic Press, San Diego CA, USA.

Kutiev, I., Marinov, S., Watanabe, S., 2006. Model of topside ionosphere scale height based on topside sounder data. Adv. Space Res. 37 (5), 943–950.

Meeus, J., 1985. Astronomical Formulæ for Calculators, third ed. Willmann-Bell, Richmond VA, USA.

Meeus, J., 1998. Astronomical Algorithms, second ed. Willmann-Bell, Richmond VA, USA.

Nautical Almanac Office, 1990. Almanac For Computers. United States Naval Observatory, Washington DC, USA.

Nsumei, P., Reinisch, B.W., Huang, X., Bilitza, D., 2012. New Vary-Chap profile of the topside ionosphere electron density distribution for use with the IRI model and the GIRO real time data. Radio Sci. 47, RS0L16. http://dx.doi.org/10.1029/2012RS004989.

Reinisch, B.X., Nsumei, P., Huang, X., Bilitza, D.K., 2007. Modelling the F2 topside and plasmasphere for IRI using IMAGE/RPI and ISIS data. Adv. Space Res. 39 (5), 731–738.

Reinisch, B.W., Galkin, I.A., Khmyrov, G.M., Kozlov, A.V., Bibl, K., Lisysyan, I.A., Cheney, G.P., Huang, X., Kitrosser, D.F., Paznukhov, V.V., Luo, Y., Jones, W., Stelmash, S., Hamel, R., Grochmal, J., 2009. New Digisonde for research and monitoring applications. Radio Sci. 44, RS0A24. http://dx.doi.org/10.1029/2008RS004115.

Schunk, R., Nagy, A., 2000. Ionospheres – Physics, Plasma Physics, and Chemistry. Cambridge University Press, Cambridge, UK.

Stankov, S.M., Jakowski, N., Heise, S., Muhtarov, P., Kutiev, I., Warnant, R., 2003. A new method for reconstruction of the vertical electron density distribution in the upper ionosphere and plasmasphere. J. Geophys. Res. 108 (A5), 1164. http://dx.doi.org/10.1029/2002JA009570.

Stankov, S.M., Stegen, K., Muhtarov, P., Warnant, R., 2011. Local ionospheric electron density profile reconstruction in real time from simultaneous ground-based GNSS and ionosonde measurements. Adv. Space Res. 47 (7), 1172–1180. http://dx.doi.org/10.1016/j.asr.2010.11.039.

Verhulst, T., Stankov, S.M., 2013. The topside sounder database – data screening and systematic biases. Adv. Space Res. 51 (11), 2010–2017. http://dx.doi.org/10.1016/j.asr.2012.12.023.

Verhulst, T., Stankov, S.M., 2014. Evaluation of ionospheric profilers using topside sounding data. Radio Sci. 49 (3), 181–195. http://dx.doi.org/10.1002/2013RS005263.

Verhulst, T., Stankov, S.M., 2015. Ionospheric specification with analytical profilers: evidences of non-Chapman electron density distribution in the upper ionosphere. Adv. Space Res. 55 (8), 2058–2069. http://dx.doi.org/10.1016/j.asr.2014.10.017.